Detrainment and braking of snow avalanches interacting with forests

Louis Védrine[1,2], Xingyue Li[1], and Johan Gaume[1,3]

[1]École polytechnique fédérale de Lausanne, Lausanne, Switzerland
[2]ENS Paris-Saclay, Gif-sur-Yvette, France
[3]WSL Institute for Snow and Avalanche Research SLF, Davos, Switzerland

Correspondence: Xingyue Li (xingyue_li@yeah.net)

Abstract. Mountain forests provide natural protection against avalanches. They can both prevent avalanche formation in release zones and reduce avalanche mobility in runout areas. Although the braking effect of forests has been previously explored through global statistical analyses on documented avalanches, little is known about the mechanism of snow detrainment in forests for small and medium avalanches. In this study, we investigate the detrainment and braking of snow avalanches in forested terrain, by performing three-dimensional simulations using the Material Point Method (MPM) and a large strain elastoplastic snow constitutive model based on Critical State Soil Mechanics. First, the snow internal friction is evaluated using existing field measurements based on the detrainment mass, showing the feasibility of the numerical framework and offering a reference case for further exploration of different snow types. Then, we systematically investigate the influence of snow properties and forest parameters on avalanche characteristics. Our results suggest that, for both dry and wet avalanches, the detrainment mass decreases with the square of the avalanche front velocity before it reaches a plateau value. Furthermore, the detrainment mass significantly depends on snow properties. It can be as much as ten times larger for wet snow compared to dry snow. By examining the effect of forest configurations, it is found that forest density and tree diameter have cubic and square relations with the detrainment mass, respectively. The outcomes of this study may contribute to the development of improved formulations of avalanche–forest interaction models in popular operational simulation tools and thus improve hazard assessment for alpine geophysical mass flows in forested terrain.

KEYWORDS: forest, avalanche, snow, detrainment, numerical modeling, material point method, gravitational mass movements.

1 Introduction

The expansion of human activity in mountains has increased the risk associated with snow avalanches (De Biagi et al., 2012) which threaten infrastructures and human lives. Forests can mitigate snow avalanche hazards without expensive construction of heavy protective measures like concrete dams. Hence, it is crucial to understand how forests affect the avalanche dynamic behaviour. A forest can have two protective effects against avalanches. It stabilises the snowpack in the release area (Viglietti et al., 2009) and reduces avalanche mobility in the runout zone. The second aspect has often been neglected because of the field observation that large avalanches can destroy forests with no significant deceleration (Bartelt and Stöckli, 2001). However, it

25 has been shown that for small to medium avalanches (e.g. < 10000 m^3), forests are normally not destroyed and can notably reduce the avalanche run-out distance (Teich et al., 2012a).

Predominant numerical tools for modelling snow avalanches use two-dimensional approaches, like depth-averaged avalanche dynamics model (Christen et al., 2010). This method is computationally efficient and a powerful tool for hazard mapping, but cannot directly capture the interaction between individual trees and an avalanche. Therefore, many studies have worked on 30 modeling the effect of a forest indirectly. There are mainly two approaches to simulate the protective effect of a forest against avalanches: the frictional approach and the detrainment approach (Feistl et al., 2012). The first accounts for the breakage of trees and debris entrainment by increasing the friction parameters of the Voellmy law (Voellmy, 1955) compared to open unforested terrain (Gruber and Bartelt, 2007; Takeuchi et al., 2018). The second approach is based on field observations and has a more solid physical meaning than the friction model. The mass and momentum of the snow stopped behind the trees 35 are directly removed from the flow, which naturally leads to deceleration and run-out shortening of the avalanche. The rate of detrainment is quantified with a detrainment coefficient K (Feistl et al., 2014).

The two methods can both empirically recover the reduction in mass and momentum of an avalanche in an efficient way, but may encounter difficulties and give unsatisfactory predictions in practical applications. According to Teich et al. (2012b), the friction approach is not effective for modelling small and medium avalanches in forested terrain, as the run-out distance was 40 overestimated even by using the smallest turbulent friction coefficient. The detrainment approach highly relies on the data from field avalanches, with which the detrainment coefficient K can be determined to apply the detrainment function in numerical modeling (Teich et al., 2014). Based on existing studies, both the forest type and the snow properties have a crucial effect on the detrainment coefficient K (Teich et al., 2012b, 2014). However, there is no systematic investigation on the controlling factors of the snow detrainment by forests under well-controlled conditions.

45 This study aims to quantify the amount of snow caught in forests and explore the mechanism of the detrainment, with comprehensive consideration of different avalanche features and forest configurations. We use a three-dimensional Material Point Method (3D MPM), by which the fractures, collisions, and large deformations involved in snow avalanches can be well captured (Gaume et al., 2018, 2019; Li et al., 2020, 2021). More importantly, individual trees and their interactions with snow avalanches can be explicitly modelled without relying on empirical laws. Compared to the popular two-dimensional tools for 50 modelling snow avalanches, the 3D MPM can fully resolve flow variations in all dimensions. Based on the simulations in this study, we can better understand the forest-avalanche interaction, reveal laws governing the effect of the key influencing factors on snow detrainment, and offer a basis for systematic calibration of the detrainment approach (Feistl et al., 2014) for operational purposes.

2 Methodology and setup

55 ### 2.1 Numerical method

2.1.1 The material point method (MPM)

Our simulations are performed using the Material Point Method (MPM), which is a hybrid Eulerian–Lagrangian method suitable to deal with large strains (Stomakhin et al., 2013). In MPM, Lagrangian particles are used to carry the information of position, velocity and deformation gradient, while the Eulerian grid is used to compute the equations of motion and for

60 updating the particle states. The governing equations are based on mass and momentum conservation as follows:

$$\frac{D\rho}{Dt} + \rho \nabla \boldsymbol{v} = 0, \tag{1}$$

$$\rho \frac{D\boldsymbol{v}}{Dt} = \nabla \boldsymbol{\sigma} + \rho \boldsymbol{g} = 0, \tag{2}$$

where t is time, $\boldsymbol{v}$ is velocity, ρ is density, $\boldsymbol{g}$ is the gravitational acceleration and $\boldsymbol{\sigma}$ is the Cauchy stress expressed by the

65 elasto-plastic constitutive relation:

$$\boldsymbol{\sigma} = \frac{1}{J} \frac{\partial \Psi}{\partial \mathbf{F}_E} \mathbf{F}_E^T \tag{3}$$

where Ψ is the elasto-plastic potential energy density, $\mathbf{F}_E$ is the elastic part of the deformation gradient $\mathbf{F}$ and $J = \det(\mathbf{F})$.

In this study, the transfers between particles and grid use the Affine Particle-In-Cell (APIC) method (Jiang et al., 2015). Compared to the Particle-In-Cell (PIC) and Fluid Implicit Particle (FLIP) techniques, the APIC approach allows both to stably

70 remove the numerical dissipation and to preserve angular momentum in addition to linear momentum.

2.1.2 Large-strain elastoplastic model

For modeling snow, we use the modified Cam Clay model with associative flow rule developed by Gaume et al. (2018). Given a stress $\boldsymbol{\tau}$, a mean effective stress and a deviatoric stress can be respectively obtained as $p = -\frac{1}{3}\mathrm{tr}(\boldsymbol{\tau})$ and $\boldsymbol{s} = \boldsymbol{\tau} + p\mathbf{I}$, where $\mathbf{I}$ is the identity matrix. The Mises equivalent stress can then be derived as $q = \sqrt{\frac{3}{2}\boldsymbol{s} : \boldsymbol{s}}$. The yield surface in the space of the

75 q–p is defined as:

$$y(p,q) = (1 + 2\beta)q^2 + M^2(p + \beta p_0)(p - p_0) \tag{4}$$

where β is the ratio between tensile and compressive strength and represents the cohesion, p_0 is the consolidation pressure and M is the slope of the cohesionless critical state line, which denotes the internal friction of snow. For $y(p,q) \leq 0$, the material follows the Hooke's law (St Venant-Kirchhoff Hencky strain), otherwise it behaves plastically. The hardening and softening of

80 the material are modelled by respectively expanding and shrinking the yield surface according to the law:

$$p_0 = K \sinh\left(\zeta \max(-\epsilon_v^P, 0)\right) \tag{5}$$

where ζ is the hardening factor, K is the material bulk modulus and $\epsilon_{\mathrm{v}}^{\mathrm{p}} = \log(\det(\mathbf{F}^P))$ is the volumetric plastic deformation.

2.2 Model setup
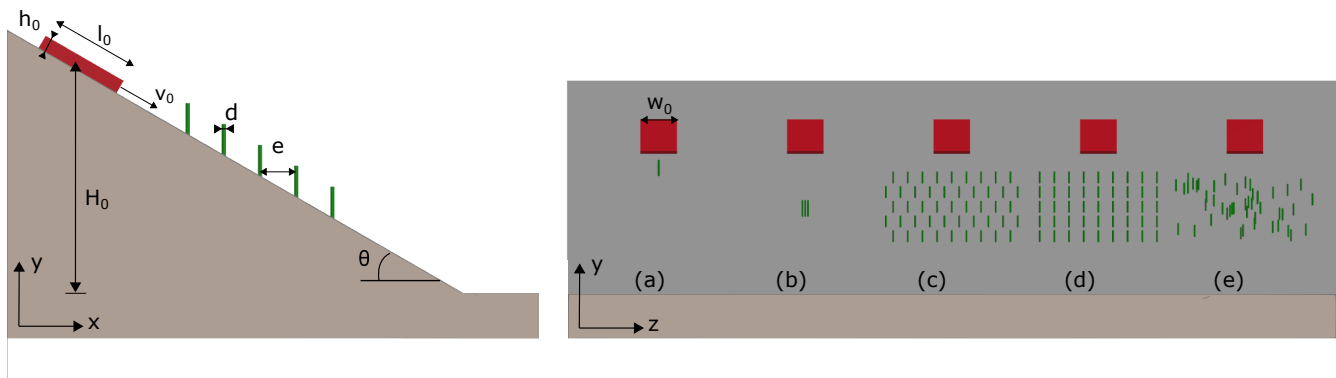
Figure 1. Model setup of MPM simulations of snow avalanches impacting to trees. The left and right are side and front views respectively. Five arrangements of trees in the right include: (a) one tree; (b) three threes; (c) regularly staggered trees; (d) regularly aligned trees; (e) random trees.

Different simplified set-ups are designed to test the protective role of different forest structures with various types of snow. As shown in the left of Fig. 1, the terrain is composed of an ideal slope with a constant inclination of $\theta = 30°$ and a horizontal deposition zone. The bed friction coefficient of the terrain is assumed to be 0.5. The snow sample is initially placed at the top of the slope at a height of $H_0 = 50.6 \mathrm{~m}$ with a prescribed initial velocity of $\boldsymbol{v}_0$. We define $h_0 = 1 \mathrm{~m}$, $l_0 = 20 \mathrm{~m}$ and $w_0 = 20 \mathrm{~m}$ as respectively the height, length, and width of the released snow. For all the snow types simulated in this study, they share the same Young's modulus ($E = 3 \mathrm{~MPa}$), Poisson's ratio ($\nu = 0.3$) and density ($\rho = 200 \mathrm{~kg/m}^3$) (Li et al., 2020). Five types of tree arrangement are designed as shown in the right of Fig. 1, including (a) one tree; (b) three threes with an identical diameter and at the same elevation; (c) a regularly staggered forest composed of trees in a staggered arrangement; (d) a regularly aligned forest composed of trees in an aligned arrangement; (e) a random forest in which trees are randomly located. All the trees are initially at the downstream of the released snow. In the setup of c)&d)&e), the width of the forests (along z) is larger than the maximum avalanche width, and the length of the forests along the flow direction is 40 m.

In addition to the different tree arrangements, the forest density ρ_{forest} and the tree diameter d are also varied to study their effect on snow detrainment. In the case of a regularly staggered forest, the forest density is controlled by the spacing between the trees e (Fig. 1). In this study, we assume that the trees are unbreakable and the trunk surface is rough. Therefore, the trees are modeled as rigid obstacles with a no-slip boundary condition. The height of the trees is set to 10 meters so that the avalanches do not overtop the trees.

In order to both well model the trees and shorten the computation time, we use a Eulerian grid size of $dx = 0.15$ m if it is not specified and 8 particles per grid. The time step is constrained by the CFL condition and the elastic wave speed to guarantee the simulation stability. The simulation data are exported every $1/12$ s.

105 ## 3 Calibration with a documented case

To calibrate the friction of snow and verify other parameters (e.g. snow density, Young's modulus, mesh size) adopted in our numerical modelling, we simulate the snow detrainment due to a group of 3 trees according to the field observation in Feistl et al. (2014). This case with 3 trees is selected for the calibration as the setup is simple and the field measurement data are available for comparison. Based on the real condition (Feistl et al., 2014), the diameter of trees is set to 1 m and the spacing

110 between trees is 0.33 m in our simulation. The simulation results are quantitatively compared with the field data in terms of the volume and height of the deposited mass (i.e. detrainment) behind the trees.

By assuming the shape of the detrainment mass as a wedge, Feistl et al. (2014) calculated the detrainment volume as

$$W = \frac{lh_{\mathrm{w}}^2}{2tan(\theta)} \tag{6}$$

with l the width of the group of trees, h_{w} the wedge height, θ the slope angle. In our simulations, the detrainment volume is

115 obtained by summarising the volume of all the particles in the detrainment mass without the assumption of the wedge shape. The height of the detrainment mass is calculated as the vertical distance from its free surface to the tree foot (as illustrated in Fig. 2). As summarised in Table 1, five simulation cases with different snow friction coefficient M were conducted, while

Table 1. Deposition height and volume of snow in simulations with different M and in the field observation

M	$W(m^3)$	$h_w(m)$
1.5	29.9	3
1.2	28.7	2.5
1	27.2	2.7
0.9	25.7	2.5
0.8	14.3	2.1
Goal (Observation)	13.85	2

all other parameters are fixed (e.g. the tension compression ratio $\beta = 0.3$, the hardening factor $\zeta = 1$, the initial consolidation pressure $p_0^{\mathrm{ini}} = 30$ kPa). With the reduction of snow friction from 1.5 to 0.8, the volume and height of the detrainment mass
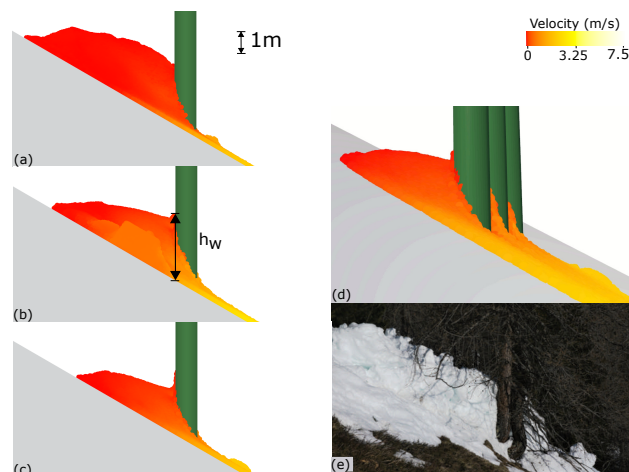
Figure 2. Side view of the snow profile stopped for different values of M: (a) M=1.2, (b) M=1, (c) M=0.8; acumulated snow behind a group of tree trees with a diameter of 1 m: (d) warm shear regime M=0.8, (e) observations (Feistl et al., 2014)

120 decreases and the case with $M = 0.8$ has a good agreement with the field data. In addition, Fig. 2 shows that the shape of the detrainment mass does not differ much with the change of snow friction. The simulation with $M = 0.8$ gives a similar profile of the detrainment mass as that observed from the field (Fig. 2d&e). This calibration case demonstrates the good feasibility of our numerical tool in capturing the key features of detrainment and serves as a reference case for the study on the effect of snow properties in the following section.

125 **4   Results**

A qualitative study of the forest-avalanche interaction will be first presented where different avalanche characteristics will be introduced (subsection 4.1). Then, the main forest factors influencing the detrainment mass in the case of a regular staggered forest will be discussed (subsection 4.2) and a newly proposed unique law for estimation of the detrainment mass will be suggested (subsection 4.3). Finally, we will show an energy investigation involving the braking process as well as the impact

130 of snow properties and forest structure (subsection 4.4).

4.1   Influence of avalanche features

4.1.1   Snow properties at the forest scale

In this study, different snow properties are adopted in the MPM modeling, representing different types of typical flow regimes of snow avalanches. The snow properties are defined by the parameters of the Modified Cam Clay model (Gaume et al.,

135 2018): the friction coefficient M, the tension compression ratio β, the hardening factor ζ and the initial consolidation pressure p_0^{ini}. Based on the calibration case reported in section 3 (Case 2 in Table 2), a more cold snow and a warmer snow are adopted
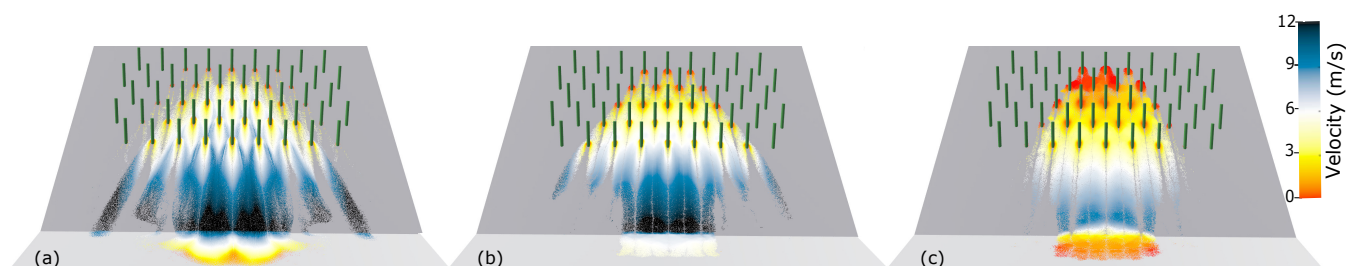
Figure 3. Flow profile for 3 different flow regimes: (a) Case 1, (b) Case 2, (c) Case 3, for a regular staggered forest at $t = 10$ s, $e = 8m$, $d = 1m$, $v_0 = 10$ m/s

Table 2. *Snow properties adopted in the MPM modeling of the flows for three typical flow regimes*

Case id	M	β	ζ	p_0^{ini}(kPa)
Case 1	0.5	0	1	3
Case 2	0.8	0.3	1	30
Case 3	1.2	0.3	1	30

respectively in Cases 1&3 (Table 2) to investigate the influence of snow properties on the avalanche-forest interaction. The cold snow in Case 1 gives a dry cohesionless granular flow with a continuous and smooth free surface, which resembles avalanches in the cold dense regime (Li et al., 2020). In comparison, the warm snow in Case 3 leads to an avalanche with granules and blocks due to the higher internal friction and cohesion, sharing features of a wet snow.

140   As illustrated in Fig. 3, a regular staggered forest is used for the three cases in Table 2. It is apparent that the snow properties have a significant effect on the accumulated snow behind the trees. Indeed, the total amount of stopped snow increases with the internal friction and the cohesion of snow. According to our simulations, some arches appear in Case 3 especially at the upstream of the avalanche. This occurrence of arches promotes the stabilization of snow on the slope and is tightly related to

145   the high internal friction and cohesion of snow.

Independent of the snow properties, there are a lot of defections as the flow front is split into many branches (Fig. 3), in contrast to the flow without forest obtained from our simulation. Fig. 3 demonstrates that the more cohesionless the snow is, the more the snow is laterally spread in the forest and gets around the trees easily. As shown by Luong et al. (2020), for the cold dense flow regime (Case 1), the snow on the side of the flow moves very fast. After being initially deflected, this lateral

150   snow moves in a diagonal channel without collision, even if a part of this effect is due to the arrangement of trees like a Galton board.
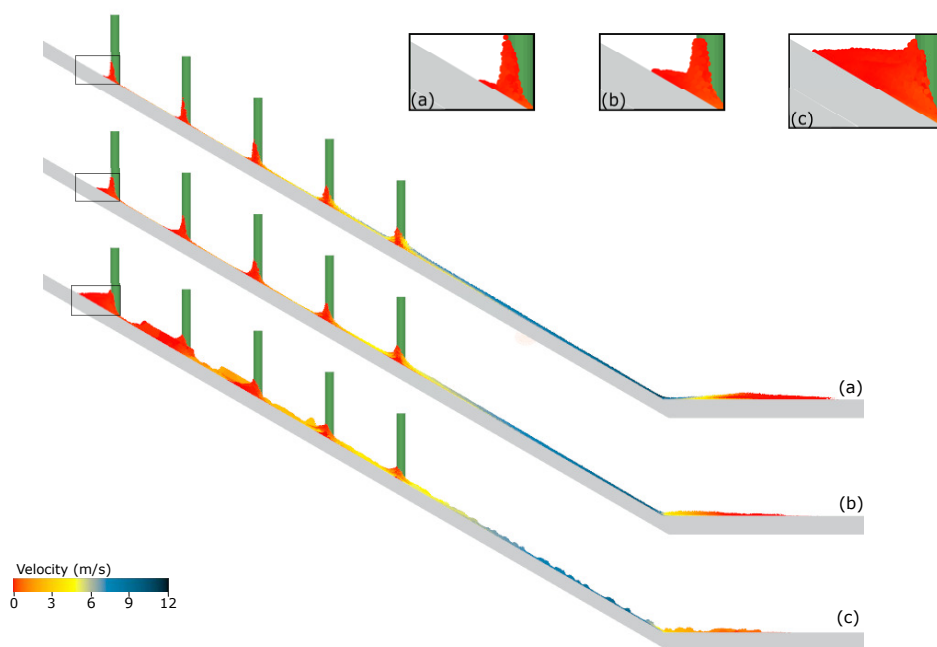
Figure 4. Profile of accumulated snow for different flow regimes: (a) Case 1, (b) Case 2, (c) Case 3, regular staggered forest at $t = 10$ s, $e = 8m$, $d = 1m$, $v_0 = 10$ m/s

In addition to the lateral motion of the avalanches, the length and height of the stopped snow are further analysed with the side view as illustrated in Fig. 4. The insets at the upper corner of Fig. 4 show the stopped mass (in red) at the uppermost trees. It is interesting to observe that the height of the wedge of stopped mass does not vary much with the different snow properties.

155 Meanwhile, the length of the snow wedge in the flow direction changes notably. With the more cohesive and frictional snow from Case 1 to Case 3, the length of the wedge increases and its free surface becomes more horizontal (inset c). According to Fig. 4, the snow properties also affect the evolution of stopped mass along the flow direction. While the shapes of the snow wedges appear to be similar along the slope in Cases 1&2, the profile of the snow changes significantly in Case 3. As blocks and granules exist in Case 3, there is more snow stopped by the trees at the upstream. It is noticed that the uppermost trees in

160 Case 3 have less stopped mass than the second uppermost trees, mainly due to the severe initial impact of the avalanche on the uppermost trees.

4.1.2 Avalanche velocity

To define the detrainment mass stopped by the trees, a criteria based on the evolution of particle velocity is used. If a snow particle has a velocity smaller than 0.5 m/s throughout the flowing process, it is considered as stopped and detrained. This

165 definition borrows the concept by Feistl et al. (2014), where the snow is directly removed from the avalanche mass once it is stopped.
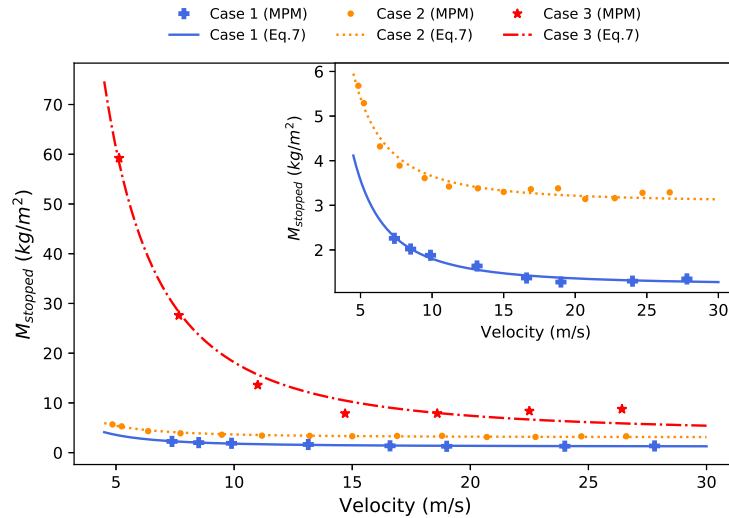
Figure 5. Evolution of the detrainment mass per unit of area of snow with the velocity (regular staggered forest, $e = 8\text{m}$)

The impact of avalanche velocity on detrainment snow is studied by imposing an initial velocity v_0 ranging from 0 to $24\,\text{m/s}$. Figure 5 shows the evolution of the detrainment mass with the front velocity at the entrance of the forest for the different snow properties (in subsection 4.1.1). The mass per unit area is calculated by dividing the total detrainment mass by the total area of influence. The latter is obtained by multiplying the number of trees with snow accumulation by the area of influence of each tree (e^2).

Firstly, the evolution of the stopped snow with snow properties is quantified in Fig.5, a very strong impact is observed, for low speeds, between the Case 1 and 3, the total amount of snow stopped is multiplied by 10. However, for each type of snow the same behaviour is observed, the detrainment mass decreases when the velocity increases and tends to a constant value for high velocities. The initial negative correlation with the low velocities is in agreement with the field observation that a lower velocity leads to more stopped snow (Feistl et al., 2014). Therefore, we propose that the detrainment mass decreases with velocity square according to

$$m_\text{d}(V_\text{f}) = \frac{p_1 + p_2 . V_\text{f}^2}{V_\text{f}^2} \tag{7}$$

with $V_\text{f} = \sqrt{v_\text{xf}^2 + v_\text{yf}^2 + v_\text{zf}^2}$ the front velocity of the avalanche when it enters in the forest. The front velocity is calculated based on the velocity of the first 15% of the particle flow to eliminate the effect of scattering particles at the avalanche front. The parameters of this model ($p_1(\text{kg/s}^2)$, $p_2(\text{kg/m}^2)$) (Fig. 5) are identified based on least squares method (Tab. 3) and both depend on the snow properties. p_2 represents the detrainment mass reached for very high velocities (Eq. 7), it is the mass stopped independently of the velocity.

Similar to the effect of velocity on the detrainment mass, Kyburz et al. (2020) showed that the impact pressure increases

185 with the velocity square. This increase of the impact pressure causes the breakage of snow during its collision with the trees, which leads to a lower volume of snow stuck behind the trees. The mass stopped for the highest velocity is rather due to the type of snow, this part of snow is initially compacted against the trunk at the front of the avalanche and is not impacted by the velocity.

4.2 Influence of forest parameters

190 ### 4.2.1 Tree diameter

The impact of tree diameter is studied for the one tree configuration with a mesh size of 0.1 m for a better modeling of thin trees. For all the snow properties, both the maximum and the final masses stopped have the same evolution trend with the tree diameter (Fig. 6). Feistl et al. (2014) proposed the following cubic model for the detrainment volume W induced by single-tree interaction:

195 $$W = \frac{d^3}{12.tan(\theta).tan(\delta/2)^2} \tag{8}$$

with d the diameter of the tree, θ the slope angle, δ the top wedge angle of the pyramid formed by stopped snow. Comparing
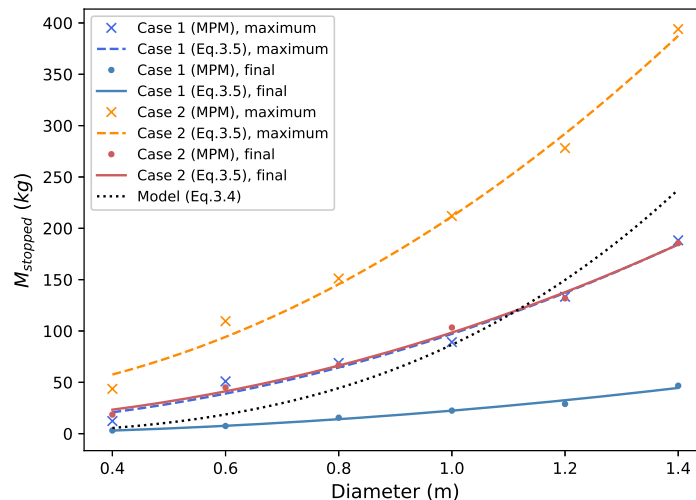
Figure 6. Evolution of the detrainment mass observed for the one tree arrangement and the fits with the tree diameter for 2 flow regimes : Case 1 and Case 2 with respectively a front velocity of 12.5 m/s and 10.6 m/s, 'maximum' refer to the maximum mass stored behind the tree and 'final' refer to the final mass stored. A slope of $30°$, and a top wedge angle of $60°$ (from measurements Feistl et al. (2014)) is used for the theoretical model (Eq. 8)

the simulated final mass with the previous analytical proposal of Feistl et al. (2014), we can notice that this model is close to

the flow in Case 2 calibrated for a tree diameter of 1 meter, it proves that the calibration is consistent. However, the numerical result shows that the order 3 model in Eq. 8 is not verified. This observation is in accordance with the analysis of the shape of the snow wedge behind the tree, indeed the height of the wedge is not linearly impacted by the tree diameter, whereas the diameter has a large impact on the length and the width of the wedge. Thus, the evolution of the stopped mass with the tree diameter follows a square law.
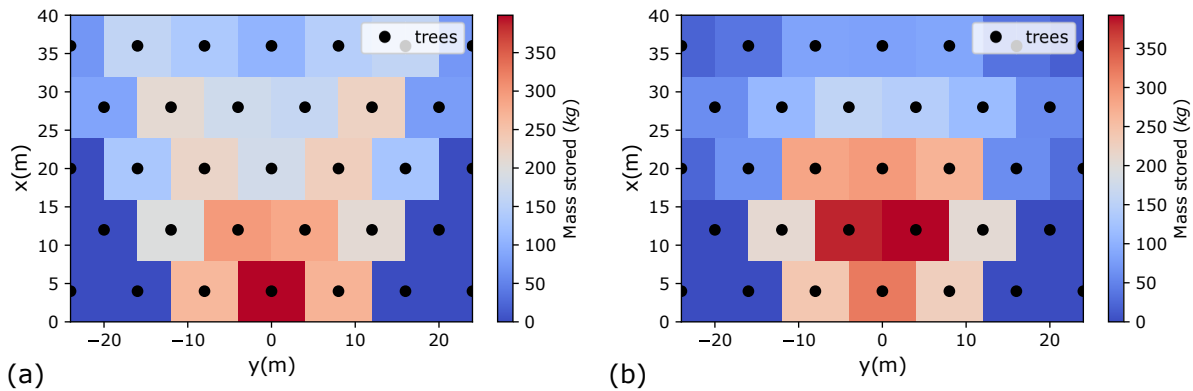
Figure 7. Distribution of the maximum detrainment mass behind each tree during the avalanche (regular staggered forest, $d = 1$m, $e = 5.5$ m), a) $v_0 = 10$ m/s, b) $v_0 = 22$ m/s

While we dispose of the evolution of the detrainment mass with the tree diameter for the one tree arrangement, in the case of an arrangement of several trees, the spatial distribution of the detrainment mass shows that trees interact with each other (Fig. 7). Comparing to the one tree result, more snow is stopped for the first row than for the one tree case, and for the lower rows the detrainment mass can be either underestimated or overestimated. This is not only a geometric effect, because the pattern of the spatial distribution of detrainment mass behind each tree depends on the velocity (Fig. 7). Thus, it reveals the difficulty to predict the distribution of detrainment mass. For a better understanding of the phenomenon, the study must be carried out at the forest scale, and the study of the forest density would help to consider the collective behavior and interaction of the trees.

For the study of a forest, the influence of tree diameter is examined by keeping the same forest density and changing the forest cover $\Phi = \frac{A_{\text{trunk}}}{A_{\text{forest}}}$, where A_{trunk} is the total area occupied by the trunks and A_{forest} the total forest area. Figure 8 depicts that the same behaviour is observed for different velocities and snow properties, and the trend is similar to the case of one tree. These results suggest that the detrainment mass evolves according to a square law with the tree diameter (Eq.(9)), with p_4 and $p_5(1/\text{m}^2)$ evaluated based on least squares method (Tab. 3).

$$m_d(V_f, d) = m_d(V_f) \cdot \left(p_3 + p_4 \cdot d^2\right) \tag{9}$$
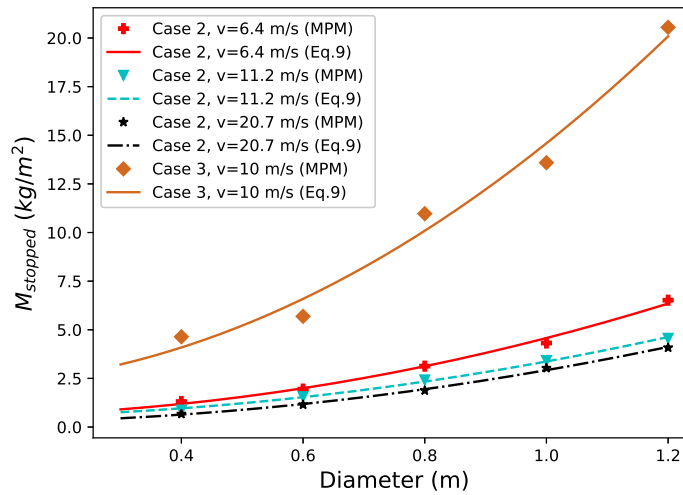
Figure 8. Evolution of the detrainment mass per unit of area with the tree diameter for different types of snow and front velocity (regular staggered forest, $e = 8$ m)

4.2.2 Forest density

Figure 9 shows the evolution of the detrainment mass under the effect of the forest density, for different front velocities. In previous models (Feistl, 2015), it was assumed that the increase of the forest density only increases the number of trees/obstacles and consequently the number of wedges, which led to a linear law between the mass stopped and the forest density. However, 220 our results suggest that the forest density has an impact on the stopped mass behind each individual tree. Indeed, compared to a forest with a lower density, a denser forest leads to more detrainment not only because there are more trees but also due to more stopped mass for each tree as snow jamming occurs. This increased detrainment due to the collective behavior of the trees is observed for all the different velocities simulated. The proposed law in Eq. 9 can be improved with consideration of the effect of forest density accoring to Eq. 10 below

225 $$m_d(V_f, d, \rho_{\text{forest}}) = m_d(V_f, d) . \left(p_5 + p_6 . \rho_{\text{forest}}^3 \right) \tag{10}$$

with p_5 and $p_6 (\text{ha}^3/\text{trees}^3)$ evaluated based on least squares method (Tab. 3).
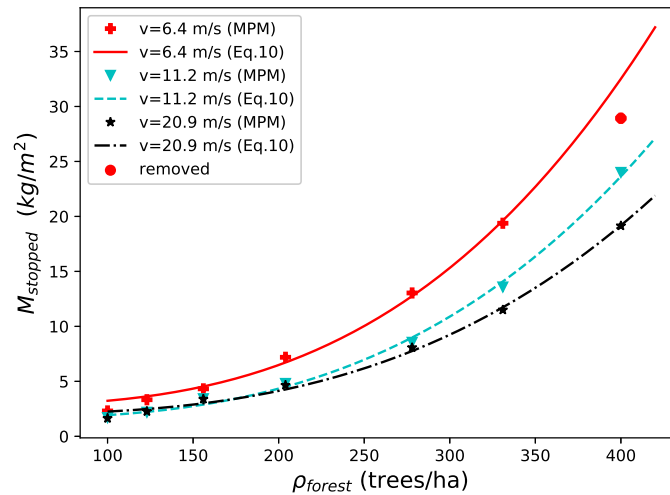
Figure 9. Evolution of the detrainment mass per unit of area with the forest density for different front velocities (regular staggered forest, snow properties: case 2, $d = 1$ m). The removed point denotes a special case not considered in the proposed cubic relation in Eq. 10, since the entire avalanche in this case is stopped due to the low flow velocity and the high forest density.

4.3 Model for detrainment mass

Based on the systematic study of the impact of the avalanche features and forest parameters, a model for the detrainment mass per unit of area can be proposed for a regular staggered forest (Eq. 11).

230
$$m_d(V_f, d, \rho_{\text{forest}}) = \frac{p_1 + p_2.V_f^2}{V_f^2} . \left(p_3 + p_4.d^2\right) . \left(p_5 + p_6.\rho_{\text{forest}}^3\right) \tag{11}$$

with V_f the frontal velocity of the avalanche when it reaches the forest, $\rho_{\text{forest}}(\text{trees/ha})$ the number of trees per hectare, d the tree diameter, and $p_{[1,2,3,4,5,6]}$ the model parameters given in Table 3.

Table 3. Parameter value of the law (11) for different snow properties (Table 2)

Type of snow	$p_1(\text{kg/s}^2)$	$p_2(\text{kg/m}^2)$	p_3	$p_4(1/\text{m}^2)$	p_5	$p_6(\text{ha}^3/\text{trees}^3)$
Case 1	58.7	1.2	0.12	0.84	4.73×10^{-1}	8.6×10^{-8}
Case 2	58	3.1	0.12	0.84	4.73×10^{-1}	8.6×10^{-8}
Case 3	1434	3.8	0.12	0.84	4.73×10^{-1}	8.6×10^{-8}

Figure 10 depicts the evolution of the detrainment mass predicted from Eq. 11 and that from MPM simulations, showing that the developed law in Eq. 11 predicts well the detrainment mass.
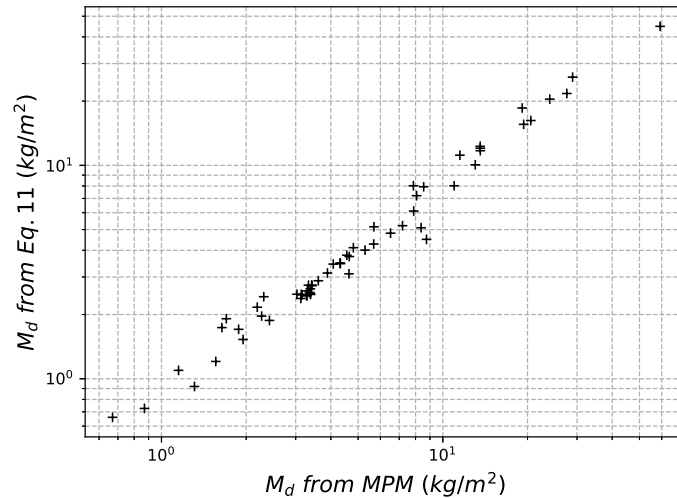
Figure 10. Evolution of the detrainment mass predicted with the model (Eq. 11) and with the observation, r^2=0.9926

4.4 Energy analysis of the avalanche–forest interaction

4.4.1 Evolution of energy and energy dissipation

After the evaluation of the detrainment mass, it is needed to quantify the impact of the detrainment process in the braking effect of forest against avalanches. To understand the physical process of the braking effect, the analysis of the evolution of the kinetic and potential energy with and without forest is made (Fig. 11). As expected, we observe when the avalanche enters the forest that the kinetic energy decreases while without forest the kinetic energy continues to increase steadily. An important difference of kinetic energy between the simulation with and without forest on the bottom of the slope ($t = 9$ s) is observed, which confirms the significant braking effect of forest. In addition, in term of potential energy, whereas the potential energy without forest decreases linearly, with forest, due to the mass which stays on the slope, the potential energy decreases more slowly and at the end of the simulation, the potential energy does not vanish due to the detrainment mass.

To understand the kinetic energy loss with the forest, two physical processes are considered, namely, detrainment and dissipation. First, a detrainment behavior accounts for the stopped snow mass behind the trees, whose potential energy is not converted to kinetic energy. Considering the avalanche potential energy with and without forest E_{pf} and E_{p0} respectively, the change of the potential energy due to the detrainment with the presence of the forest E_{pd} can be defined as

$$E_{pd} = E_{pf} - E_{p0}. \tag{12}$$
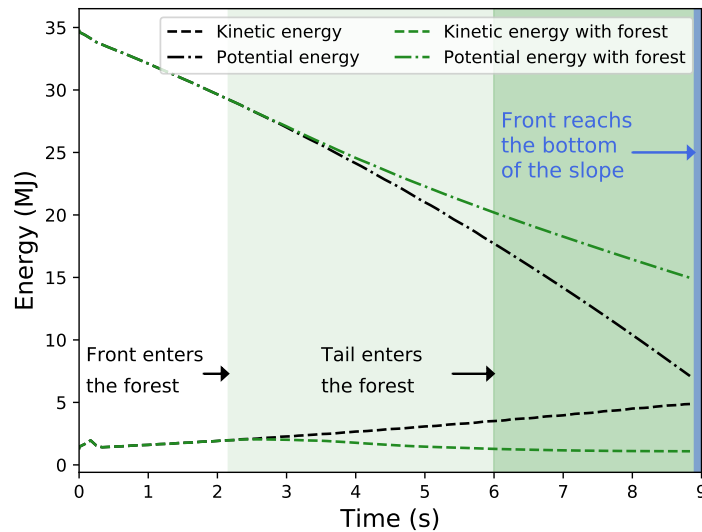
Figure 11. Temporal evolution of the kinetic and potential energy without forest and with a regular staggered forest (Case 2, $v_0 = 6$ m/s)

250 Secondly, the dissipation process is associated with avalanche-tree interactions including collision and friction, which lead to plastic dissipation and random fluctuation. This dissipation due to the trees is defined as $\tilde{E}_f$, whose calculation is detailed in Appendix A.

Figure 12 shows the energy change due to the detrainment and dissipation processes (i.e. E_{pd} and $\tilde{E}_f$), which contribute to the reduction of the avalanche kinetic energy with the forest. Taking the avalanche with forest as a reference, when its front

255 enters the forest, the energy loss due to detrainment and dissipation start to grow (at around 2.3 s in Fig. 12). The increasing rate of $\tilde{E}_f$ tends to decrease with time, as the velocity of the flow decreases (see the kinetic energy in Fig. 11) and the dissipation by ground friction reduces. In contrast, the growth rate of E_{pd} increases with time. Indeed, after small wedges are formed behind and around the trees, the spacing between trees decreases, which leads to faster blockage of incoming snow particles. It should be noted that the forest enhances energy loss due to detrainment and dissipation, but meanwhile reduces the avalanche velocity.

260 Hence, the presence of the forest leads to lower energy dissipation due to ground friction, as it is positively correlated with the avalanche velocity.

4.4.2 Impact of the forest structure and the snow properties on the energy loss

The same experiment is carried out for three types of snow (Table 2) and three types of forest (regular aligned, regular staggered and random) with the same forest density and tree diameter, in order to analyse the separate processes of detrainment and

265 dissipation. Figure 13 depicts the detrainment and dissipation energies when the front of the avalanche reaches the bottom of the slope. It reveals that the detrainment represents a larger part of the energy loss compared to the dissipation. The detrainment
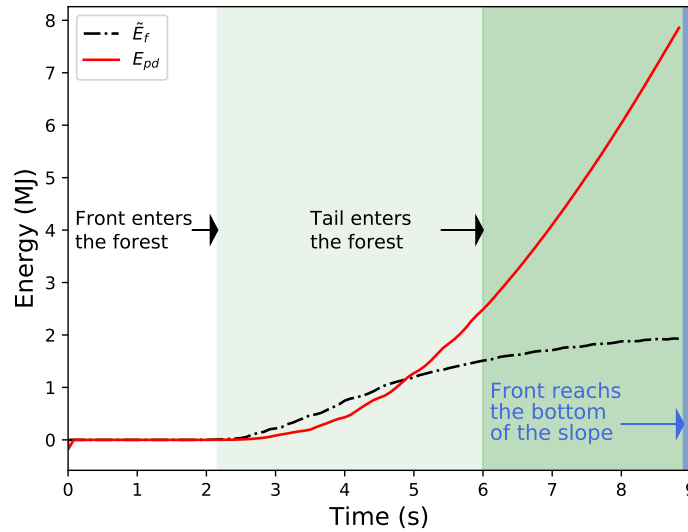
Figure 12. Temporal evolution of the detrainment energy and dissipation due to the forest (Case 2, $v_0 = 6$ m/s)
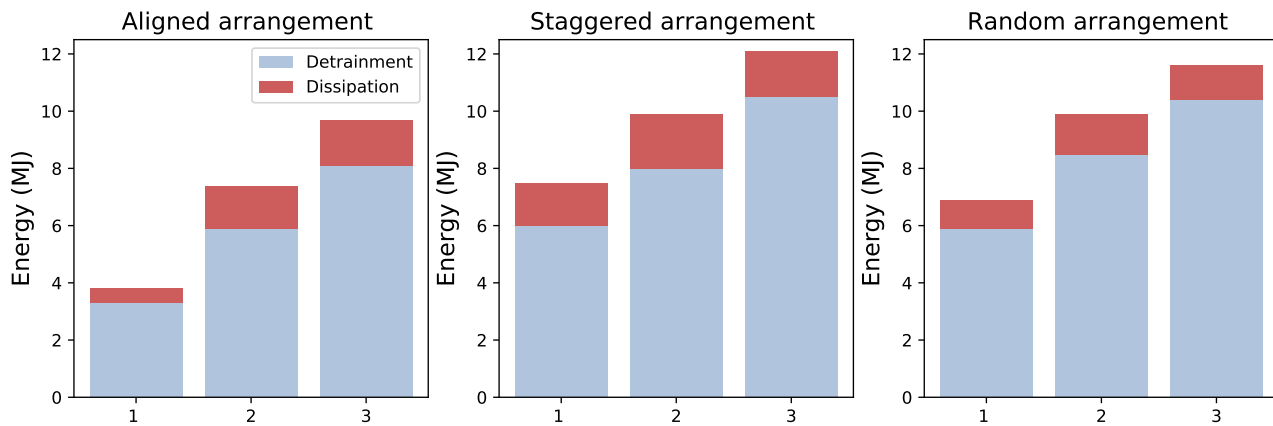
Figure 13. Energy detrainment and dissipation for different snow properties (1: case 1, 2: case 2, 3: case 3 with M=1) and for 3 types of forest structure (regular aligned, regular staggered and random)

increases with the cohesion and the internal friction of snow, whereas the dissipation due to forest changes slightly with the snow properties. For the three types of snow, the dissipation is higher for the regular staggered forest, due to the Galton board arrangement for which collisions and deflections are more frequent.The most notable difference for the different forest arrangements in Fig. 13 is that much lower detrainment is observed for the aligned forest, indicating that much less snow is stopped. Indeed, when trees are regularly aligned, a large part of the flow passes through the space between trees without

270

collisions (Fig. 14). These results suggest that in the case of a regular forest, the staggered arrangement should be privileged for a better protective effect. The detrainment energy when the avalanche reaches the bottom of the slope is similar between the random and the regular staggered arrangements.

275   Given the same snow properties (e.g. Case 2), the final stopped mass with the aligned, staggered, and random arrangements is 2147 kg, 3002 kg, and 13061 kg respectively. The same trend is observed for other considered snow properties in this study (Cases 1&3). Compared to the regular aligned forest, the regular staggered forest stops more snow due to a smaller spacing (along the diagonal direction) between the trees (Fig. 14a&b). The random arrangement gives the highest stopped mass, as each tree cluster serves as a dam and collectively block a large amount of snow (Fig. 14c). Consequently, in term of the final

280 run-out distance, the avalanche in the random forest travels a shorter distance than that in the regular staggered forest, which suggests that the random one has a higher protective effect.
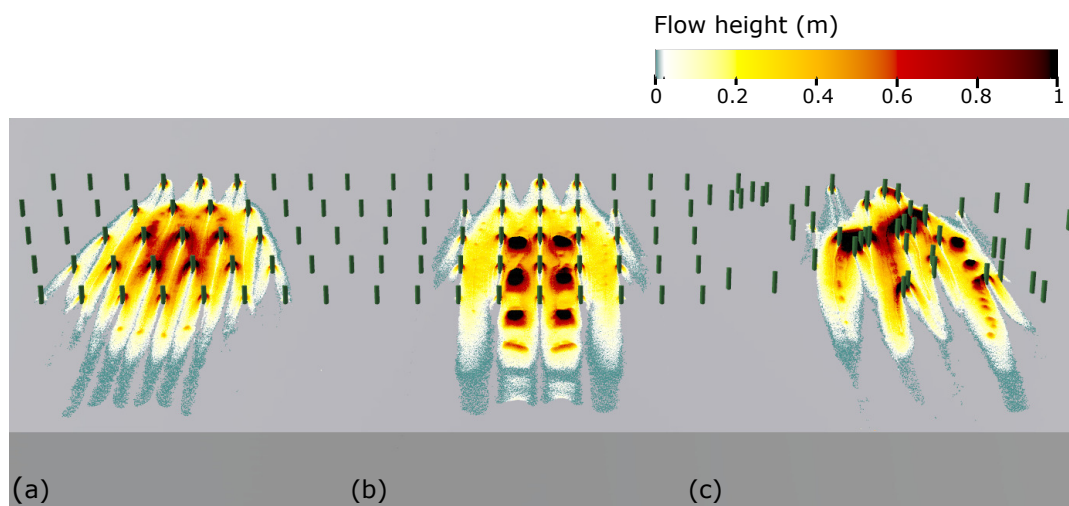
Figure 14. Flow height of the avalanche in a forest with (a) staggered arrangement, (b) aligned arrangement, (c) random arrangement, (Case 2, $v_0 = 6$ m/s, t= 9 s)

5   Discussion and conclusions

In this study, we have explored the avalanche–forest interactions with the material point method (MPM) and an elastoplastic constitutive model. The aim is to highlight the dependencies of the detrainment mass and understand the physical process of the

285 braking effect of forest with respect to avalanches dynamics. We have systematically examined the effect of snow properties, by studying both cold and wet snow. It is found that snow friction and cohesion have a large impact on detrainment mass behind the trees. Low snow friction and cohesion give fluid-like behaviour and highly sheared flows, and consequently little snow is stopped. When snow becomes more frictional and cohesive, large wedge and arches appear behind the trees, which contribute to large amount of snow stopped.

290   Interestingly, our analysis of the effect of avalanche velocity reveals that the detrainment mass decreases with the velocity and reaches a plateau value for high velocities (typically higher than $15\,\mathrm{m/s}$). While the detrainment mass linearly decreases with increasing velocity in Feistl et al. (2014), our numerical results suggest a decrease with velocity square. Knowing the relation between the detrainment mass per unit of area M_d and the detrainment coefficient $K = \frac{M_\mathrm{d} \cdot V_\mathrm{f}^2 \cdot cos(\theta)}{l_\mathrm{avalanche}}$ (Feistl, 2015) the detrainment rate can be assessed, with V_f the front velocity, θ the slope angle, $l_\mathrm{avalanche}$ the avalanche length. For an open

295   forest or old forests, Feistl et al. (2014) proposed a value of $K = 10\,\mathrm{Pa}$ independently of the snow properties and the front velocity. With our simulation results, for the case 1, we obtain a value of $K = 5.31$ for a velocity of $7.4\,\mathrm{m/s}$ and $K = 32.4$ for a velocity of $24\,\mathrm{m/s}$, while for case 2, we obtain $K = 10.1$ for a velocity of $7.7\,\mathrm{m/s}$ and $K = 86.6$ for a velocity of $24.7\,\mathrm{m/s}$. This underlines a high dependency of the detrainment coefficient on the snow properties and on the front velocity of the avalanche. The comparison with the previous value (Feistl et al., 2014) of K for an open forest suggests that it is only valid

300   for low velocities. Therefore, an implementation of our proposed velocity-based model in the detrainment approach would provide higher detrainment mass for high velocity which would therefore lead to lower run-out distance and velocities.

    In addition, we have examined different forest arrangements, by varying the forest density and the tree diameter, which both can easily be identified from a forest inventory. It is found that the detrainment mass increases with the cube of forest density and the square of tree diameter. Contrary to the geometric model proposed by Feistl et al. (2014), we found that the height of

305   the wedge does not vary linearly with the tree diameter. This comprehensive numerical investigation allowed us to propose a unified law for the detrainment mass (Eq. 11). Therefore, it enables an estimation of the K value as show before, which may serve as an input to 2D depth-averaged methods to better predict the detrainment mass.

    From an energy point of view, our results suggest that the detrainment has the largest impact on the energy loss, which claims the use of the detrainment approach. However, the additional dissipation due to forest ($\tilde{E}_\mathrm{f}$) is not negligible, although that the

310   detrainment approach removes not only the potential energy of the removed particles but also their kinetic energy. In view of the kinetic energy levels compared to the dissipation added with forest, the kinetic energy of the particles removed seems too low to represent the dissipation added with forest. This result implies that an increase of the bed friction in combination to the detrainment approach could be justified to take into account the increase in energy dissipation linked to the effect of forest.

    The presented research focuses on examining the interaction between forest and avalanches with idealised conditions, which

315   enable to give new outlooks for further studies. Here, trees are modeled as rigid obstacles and with a no-slip boundary condition. Hence, this study is only valid for small to medium avalanches where the forest is not destroyed, and the trees act as obstacles. Secondly taking into account the true friction coefficient of the tree would allow, as suggested by Teich et al. (2014), to define a law for different species. Another limitation is the consideration of an ideal slope with a constant inclination. This could be further changed to any other shape to be more realistic and other tree arrangements could be explored as well. It would also

320   be interesting to study longer forest with larger released volumes, to obtain longer permanent regimes, this would however significantly increase the computational time.

    Despite the assumptions and idealisation applied in this study, it highlights the main factors influencing the detrainment mass in an unique law depending on snow mechanical properties, front velocity, and forest parameters. This outcome of this work can be applied not only for calibration of depth-averaged models used operationally (e.g., Christen et al. (2010)), but also for

325 forest management. Moreover, according to energy analysis, a good calibration of the detrainment approach seems to be not enough to model all processes driving avalanche-forest interaction. This suggests that an approach combining detrainment and friction increase could be more appropriate. Finally, although this study focused on snow avalanches, the methods used and the general relationships found are also relevant to other geophysical mass flows interacting with forests and can pose strong impacts on hazard assessment and risk management.

330   *Code and data availability.*   All the data used in the figures in this paper are on Zenodo at https://doi.org/10.5281/zenodo.5547395. A detailed description of the MPM model can be found in a previous publication at https://www.nature.com/articles/s41467-018-05181-w.

Video supplement.   Videos of the simulations presented in Figs. 2, 3, 4 and 14 are available on Zenodo at https://doi.org/10.5281/zenodo.5547386.

Appendix A: Calculation of energy dissipation due to forest

By defining Δe the additional dissipation at each time step, it is possible to separate it into two parts (Li et al., 2020): the
335   dissipation inside the flow w_{int} and through the boundary bed w_b, and in the case with forest, the dissipation $\tilde{e}_f$ is added. Hence, the total dissipation in the case without forest is $\Delta e_0 = w_{b_0} + w_{int_0} \approx w_{b_0}$, as the internal dissipation can be negligible compared to the bed friction dissipation (Li et al., 2020). Similarly, in the forest case $\Delta e_f = w_{b_f} + w_{int_f} + \tilde{e}_f \approx w_{b_f} + \tilde{e}_f$.

As the velocity of the avalanche is reduced with forest, the frictional dissipation with the ground decreases, to evaluate the dissipation added with forest, we can not simply substract the dissipation obtained with and without forest. Therefore we use
340   the equation A1a which allows us to calculate $\tilde{E}_f$ based on our simulations. Indeed, by replacing the expression of Δe_0 and Δe_f (Eq. A1b), and by assuming that the bed dissipation w_b depends linearly on the velocity (i.e $\frac{w_{b_f}(i.\Delta t)}{v_f(i.\Delta t)} \approx \frac{w_{b_0}(i.\Delta t)}{v_0(i.\Delta t)}$) (Eq. A1b), the definition of the dissipation added due to forest is obtained (Eq. A1c). So at the time step n, with Δt the time step, it is possible to obtain the total dissipation added by the forest $\tilde{E}_f$.

$$\sum_{i=0}^{n-1} \left(\frac{\Delta e_f(i.\Delta t)}{v_f(i.\Delta t)} - \frac{\Delta e_0(i.\Delta t)}{v_0(i.\Delta t)} \right).v_f(i.\Delta t) \tag{A1a}$$

345    $$= \sum_{i=0}^{n-1} \left(\frac{w_{b_f}(i.\Delta t) + \tilde{e}_f(i.\Delta t)}{v_f(i.\Delta t)} - \frac{w_{b_0}(i.\Delta t)}{v_0(i.\Delta t)} \right).v_f(i.\Delta t) \tag{A1b}$$

$$\approx \sum_{i=0}^{n-1} \tilde{e}_f(i.\Delta t) \tag{A1c}$$

$$= \tilde{E}_f(n.\Delta t) \tag{A1d}$$

Author contributions.   L.V. performed the simulations, made the figures and videos, analyzed the results and wrote the paper under the supervision of X.L. and J.G. X.L. prepared the numerical setup of the simulations. J.G. designed the study and obtained the funding. All
350   authors were involved in the writing of the manuscript and physical interpretation of the results.

Competing interests.   The authors declare that they have no conflict of interest.

Acknowledgements. We acknowledge Dr. Perry Bartelt and Dr. Peter Bebi from SLF, Davos for insightful discussions on the topic of avalanche - forest interaction and the detrainment approach. We also thank Jean-Louis Gay from the Vaud Canton, Clara Streule and Francesc Molné from EPFL for their preliminary contribution on the topic in the framework of an EPFL Design Project motivated by a forest fire in an
355   avalanche-prone area (Les Diablerets). Finally, we thank Dr. Martin Proksch from the Wallis canton and Andreas Tegethoff from Geoformer for constructive suggestions for the practical application of this work. Johan Gaume acknowledges funding from the Swiss National Science Foundation (Eccellenza project: grant number PCEFP2_181227; SPARK project grant number CRSK-2_195914).

References

Bartelt, P. and Stöckli, V.: The influence of tree and branch fracture, overturning and debris entrainment on snow avalanche flow, Annals of
360   Glaciology, 32, 209–216, https://doi.org/10.3189/172756401781819544, 2001.

Christen, M., Kowalski, J., and Bartelt, P.: RAMMS: Numerical simulation of dense snow avalanches in three-dimensional terrain, Cold
    Regions Science and Technology, 63, 1–14, https://doi.org/https://doi.org/10.1016/j.coldregions.2010.04.005, 2010.

De Biagi, V., Frigo, B., and Chiaia, B.: VULNERABILITY OF BUILDINGS AGAINST AVALANCHE HAZARD, 2012.

Feistl, T.: Vegetation effects on avalanche dynamics, Ph.D. thesis, 2015.

365 Feistl, T., Bebi, P., Bühler, Y., Christen, M., Teich, M., and Bartelt, P.: Stopping behavior of snow avalanches in forests, in: Proceedings of
    the International Snow Science Workshop ISSW. Anchorage, Alaska, pp. 420–426, 2012.

Feistl, T., Bebi, P., Teich, M., Bühler, Y., Christen, M., Thuro, K., and Bartelt, P.: Observations and modeling of the braking effect of forests
    on small and medium avalanches, Journal of Glaciology, 60, 124–138, https://doi.org/10.3189/2014JoG13J055, 2014.

Gaume, J., Gast, T., Teran, J., van Herwijnen, A., and Jiang, C.: Dynamic anticrack propagation in snow, Nature Communications, 9,
370   https://doi.org/10.1038/s41467-018-05181-w, 2018.

Gaume, J., van Herwijnen, A., Gast, T., Teran, J., and Jiang, C.: Investigating the release and flow of snow avalanches at the
    slope-scale using a unified model based on the material point method, Cold Regions Science and Technology, 168, 102 847,
    https://doi.org/https://doi.org/10.1016/j.coldregions.2019.102847, 2019.

Gruber, U. and Bartelt, P.: Snow avalanche hazard modelling of large areas using shallow water numerical methods and GIS, Environ-
375   mental Modelling Software, 22, 1472–1481, https://doi.org/https://doi.org/10.1016/j.envsoft.2007.01.001, modelling, computer-assisted
    simulations, and mapping of dangerous phenomena for hazard assessment, 2007.

Jiang, C., Schroeder, C., Selle, A., Teran, J., and Stomakhin, A.: The Affine Particle-in-Cell Method, ACM Trans. Graph., 34,
    https://doi.org/10.1145/2766996, 2015.

Kyburz, M., Sovilla, B., Gaume, J., and Ancey, C.: Decoupling the Role of Inertia, Friction, and Cohesion in Dense Granular Avalanche
380   Pressure Build-up on Obstacles, Journal of Geophysical Research: Earth Surface, 125, https://doi.org/10.1029/2019JF005192, 2020.

Li, X., Sovilla, B., Jiang, C., and Gaume, J.: The mechanical origin of snow avalanche dynamics
    and flow regime transitions, The Cryosphere, 14, 3381–3398, https://doi.org/10.5194/tc-14-3381-2020, 2020.

Li, X., Sovilla, B., Jiang, C., and Gaume, J.: Three-dimensional and real-scale modeling of flow regimes in dense snow avalanches, Land-
    slides, https://doi.org/10.1007/s10346-021-01692-8, 2021.

385 Luong, T. T. H., Baker, J., and Einav, I.: Spread-out and slow-down of granular flows through model forests, Granular Matter, 22, 15, 2020.

Stomakhin, A., Schroeder, C., Chai, L., Teran, J., and Selle, A.: A Material Point Method for Snow Simulation, ACM Trans. Graph., 32,
    https://doi.org/10.1145/2461912.2461948, 2013.

Takeuchi, Y., Nishimura, K., and Patra, A.: Observations and numerical simulations of the braking effect of forests on large-scale avalanches,
    Annals of Glaciology, 59, 50–58, https://doi.org/10.1017/aog.2018.22, 2018.

390 Teich, M., Bartelt, P., Grêt-Regamey, A., and Bebi, P.: Snow Avalanches in Forested Terrain: Influence of Forest Parameters, Topography,
    and Avalanche Characteristics on Runout Distance, Arctic, Antarctic, and Alpine Research, 44, 509 – 519, https://doi.org/10.1657/1938-
    4246-44.4.509, 2012a.

Teich, M., Vasella, I., Bartelt, P., Bebi, P., Feistl, T., and Grêt, A.: AVALANCHE SIMULATIONS IN FORESTED TERRAIN: A FRAME-
    WORK TOWARDS A BAYESIAN PROBABILISTIC MODEL CALIBRATION, 2012b.

395   Teich, M., Fischer, J.-T., Feistl, T., Bebi, P., Christen, M., and Grêt-Regamey, A.: Computational snow avalanche simulation in forested terrain, Natural Hazards and Earth System Sciences, 14, 2233–2248, https://doi.org/10.5194/nhess-14-2233-2014, 2014.

Viglietti, D., Letey, S., Motta, R., Maggioni, M., and Freppaz, M.: Snow and avalanche: The influence of forest on snowpack stability, ISSW 09 - International Snow Science Workshop, Proceedings, pp. 323–327, 2009.

Voellmy, A.: Uber die Zerstorungskraft von Lawinen., Schweizerische Bauzeitung, Jahrg., 73, 159–162, 1955.